Phenoxazine-based COFs for CO_2/N_2 Separation and Organic Dye Adsorption

Yi-Fan Liu, Lan Yang, Xinyu Shen, Jie Zhao, Yamin He and Ru-Yi Zou*

Table of Contents

1. Synthesis of linkers

1.1 Synthesis of 2,4,6-tris(4-bromophenyl)-1,3,5-triazine

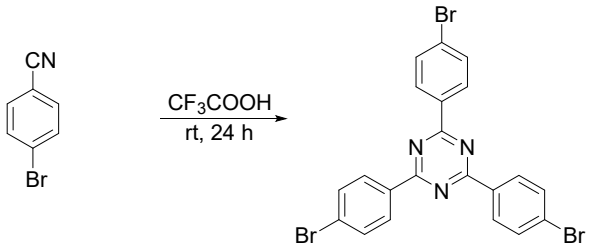

2,4,6-tris(4-bromophenyl)-1,3,5-triazine was synthesized following a previously reported procedure.[1] To an oven-dried two-necked flask equipped with a magnetic stirrer was added 4-bromobenzonitrile (5 g, 27.5 mmol), then 10 mL of CF_3SO_3H was slowly added dropwise to the system. After stirring the reaction for 24 h at the room temperature, an orange-yellow liquid was obtained. The resulting liquid was then poured into 50 mL of deionized water and neutralized with ammonia, resulting in the formation of a white suspension. The suspension was filtered, and the filter cake was thoroughly washed with deionized water and methanol. The washed filter cake was collected, yielding a white solid product weighing 4.45 g. Yield: 89%.

^{1}H NMR (400 MHz, $CDCl_3$): δ (ppm) 8.60 (d, J = 8.32 Hz, 6H, Ph-*H*), 7.71 (d, J = 8.16 Hz, 6H, Ph-*H*), 1.54 (H_2O)[2] (Fig. S14).

1.2 Synthesis of 4',4''',4''''''-(1,3,5-triazine-2,4,6-triyl)tris(3-hydroxy-[1,1'-biphenyl]-4-carbaldehyde)

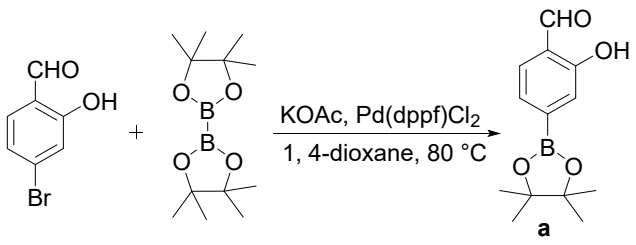

Compound **a** was synthesized following a previously reported procedure.[3] In a 100 mL round-bottom flask, 4-bromosalicylaldehyde (1.8 g, 9 mmol), bis(pinacolato)diboron (2.4 g,

9.45 mmol), KOAc (2.65 g, 27 mmol), and 55 mL of dioxane were combined. The flask was evacuated and purged with N_2 three times. Then, $Pd(dppf)Cl_2$ (0.2 g, 3% mmol) was added under a N_2 atmosphere and the mixture was heated at 80 °C for 8 h. After cooling to room temperature, the resulting suspension was filtered. The filtrate was then collected and subjected to purification by column chromatography (PE: EA = 25: 1), yielding a white flaky solid weighing 1.63 g. Yield: 73%.

^{1}H NMR (400 MHz, $CDCl_3$): δ(ppm) 10.83 (s, 1H, -O*H*), 9.92(s, 1H, Ph-*H*), 7.55 (d, J = 8.0 Hz, 1H, Ph-*H*), 7.41 (d, 2H, Ph-*H*), 1.35 (s, 12H, -CH_3)[3] (Fig. S15).

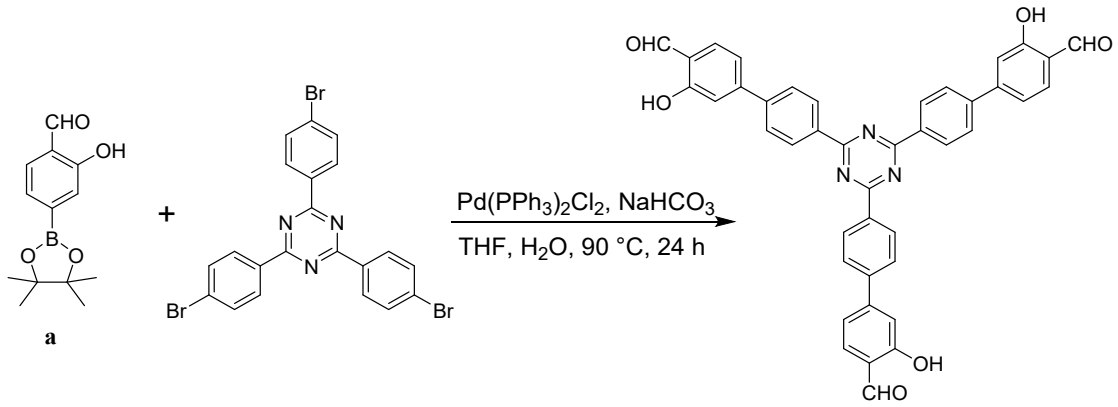

Compound **a** (0.93 g, 3.75 mmol), 2,4,6-tris(4-bromophenyl)-1,3,5-triazine (0.68 g, 1.25 mmol), and $NaHCO_3$ (0.945 g, 11.25 mmol) were added into a two-neck round-bottom flask containing a solution of 50 mL of THF and 5 mL of H_2O. The flask was then evacuated and purged with N_2 three times. Subsequently, $Pd(PPh_3)_2Cl_2$ (0.079 g, 9% mmol) was added under a N_2 atmosphere, and the mixture was heated at 90 °C for 24 h, resulting in the formation of a yellow suspension. The reaction solution was cooled to room temperature, and 1 M of HCl was added to adjust the pH to weak acidity. The suspension was filtered under reduced pressure, and the solid was washed several times with hot methanol. The resulting solid was dried under vacuum at 80 °C for 8 h, yielding a pale yellow solid weighing 0.67 g. Yield: 80%.

^{1}H NMR (400 MHz, DMSO-d_6): δ (ppm) 10.97 (s, 3H, -O*H*), 10.32 (s, 3H, -C*H*O), 8.86 (d, J = 7.4 Hz, 6H, Ph-*H*), 7.99 (d, J = 7.76 Hz, 6H, Ph-*H*), 7.82 (d, J = 7.56 Hz, 3H, Ph-*H*), 7.42 (d, J = 10.76 Hz, 6H, Ph-*H*) (Fig. S16).

Due to the limited solubility of 1,3,5-tri(3-hydroxy-4-formylphenyl)triazine, obtaining a ^{13}C NMR spectrum was challenging. To facilitate the characterization of its structure, KOH was added to the original NMR tube, enabling the sample to dissolve. The subsequent NMR analysis yielded the following results:

^{1}H NMR (400 MHz, DMSO-d_6): δ (ppm) 10.43 (s, 3H, -C*H*O), 8.35 (t, 6H, Ph-*H*), 7.63 (d, 9H, Ph-*H*), 7.29 (s, 3H, Ph-*H*), 6.99 (d, 3H, Ph-*H*), 4.79 (*H*$_2$O/KOH) (Fig. S17).

^{13}C NMR (100 MHz, DMSO-d_6): δ (ppm) 190.81, 170.49, 168.33, 146.58, 143.96, 135.05, 129.27, 128.62, 127.16, 123.95, 119.50, 114.32 (Fig. S18).

1.3 Synthesis of 4',4''',4'''''-(1,3,5-triazine-2,4,6-triyl)tris([1,1'-biphenyl]-4-carbaldehyde)

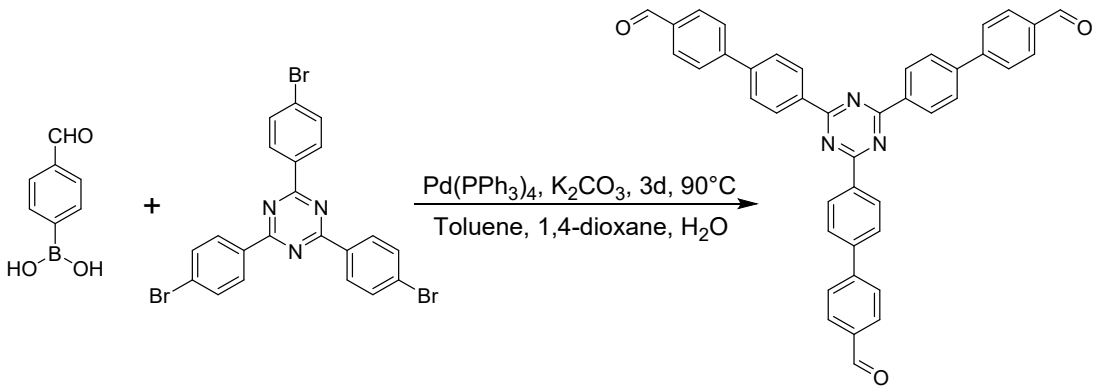

4',4''',4'''''-(1,3,5-triazine-2,4,6-triyl)tris([1,1'-biphenyl]-4-carbaldehyde) was synthesized following a previously reported procedure.[4] In a 50 mL two-neck round-bottom flask, 2,4,6-tris(4-bromophenyl)-1,3,5-triazine (0.68 g, 1.25 mmol), 4-formylphenylboronic acid (0.8 g, 5.3 mmol), K_2CO_3 (1.38 g, 10 mmol), and a mixture of 1,4-dioxane/toluene/water (20/5/2 mL) were combined. The flask was subjected to three cycles of evacuation/nitrogen purging. Subsequently, $Pd(PPh_3)_4$ (0.014 g, 1% mmol) was added, and the reaction was conducted at 90 °C for three days. After cooling to room temperature, the samples were filtered under reduced pressure and sequentially washed with acetone, water and methanol in turns. The resulting solid was dried under vacuum at 60 °C for 12 h, yielding a gray solid weighing 0.38 g. Yield: 49%.

^{1}H NMR (400 MHz, DMSO-d_6): δ (ppm) 10.11 (s, 3H, -C*H*O), 8.88 (d, J = 7.04 Hz, 6H, Ph-*H*), 8.08 (s, 18H, Ph-*H*) (Fig. S19).

1.4 Synthesis of 10- (4-aminophenyl)-3,7-phenoxazinediamine

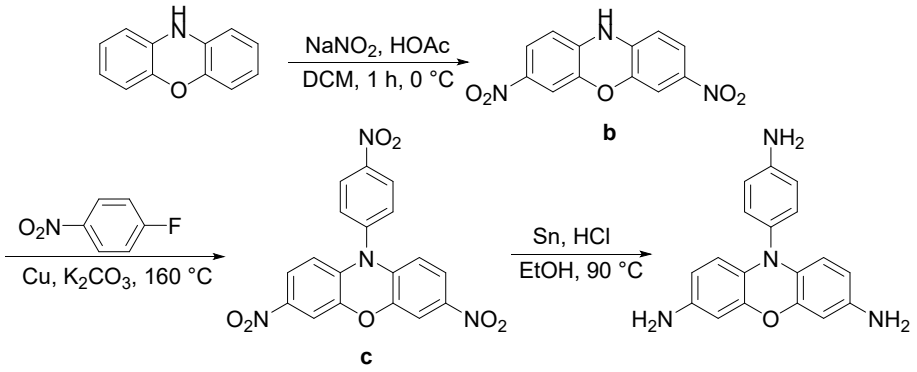

To an ice-cooled 100 mL two-necked flask were added phenoxazine (2 g, 10.9 mmol), Na_2NO_2 (3 g, 32.7 mmol), 4 mL HOAc, and 10 mL of CH_2Cl_2. After 10 mins, an additional 3 g of Na_2NO_2 (32.7 mmol), 4 mL of HOAc, and 10 mL of CH_2Cl_2 were added to the system. After 5 mins, 12 mL of HOAc was added, and stirring was continued. After 1 h, a red paste mixture was obtained. The mixture was filtered under reduced pressure, and the filter cake was washed several times with deionized water. The resulting solid was recrystallized from a hot DMF solution, filtered, and dried at 60 °C under vacuum. This yielded 2.53 g of bright red solid **b**. Yield: 85%.

^{1}H NMR (400 MHz, DMSO-d_6): δ (ppm) 10.13 (s, 1H, -N*H*-), 7.74 (dd, J = 8.72, 2.48 Hz, 2H, Ph-*H*), 7.39 (d, J = 2.48 Hz, 2H, Ph-*H*), 6.62 (d, J = 8.76 Hz, 2H, Ph-*H*), 7.96 (s, 1H, -C*H*O, DMF), 2.89 (s, 3H, -C*H*$_3$, DMF), 2.73 (s, 3H, -C*H*$_3$, DMF)[5] (Fig. S20).

In a 50 mL two-necked flask, the **b** (0.4 g, 1.46 mmol), Na_2CO_3 (0.46 g, 4.38 mmol), Cu (0.01 g, 10% mmol), and 20 mL 4-fluoronitrobenzene were combined. The flask was subjected to three cycles of evacuation and nitrogen purging before being heated at 160 °C for 24 h. After cooling the reaction system to room temperature, it was filtered and washed with CH_2Cl_2, resulting in the formation of 0.3 g of orange-red solid **c**. Yield 52%.

^{1}H NMR (400 MHz, DMSO-d_6): δ (ppm) 8.60 (d, J = 8.92 Hz, 2H, Ph-*H*), 7.92 (d, J = 8.96 Hz, 2H, Ph-*H*), 7.65 (dd, J = 8.92 Hz, 2.56 Hz, 2H, Ph-*H*), 7.59 (d, J = 2.52 Hz, 2H, Ph-*H*), 6.08 (d, J = 8.92 Hz, 2H, Ph-*H*) (Fig. S21).

The **c** (0.6 g, 1.52 mmol) and Sn (0.86 g, 7.2 mmol) were introduced into a 50 mL two-necked flask, followed by the slow dropwise addition of 15 mL HCl. The mixture was refluxed under an N_2 atmosphere for 24 h. After allowing the solution to cool to room temperature, impurities were filtered out, and the pH of the filtrate was adjusted to alkaline using a 4 M NaOH solution, resulting in the precipitation of blue-purple solids. The solid was recrystallized using THF, yielding a dark gray solid weighing 0.39 g. Yield: 84%.

^{1}H NMR (400 MHz, DMSO-d_6): δ (ppm) 6.88 (d, J = 8.24 Hz, 2H, Ph-*H*), 6.69 (d, J = 8.24 Hz, 2H, Ph-*H*), 6.03 (d, J = 1.88 Hz, 2H, Ph-*H*), 5.89 (d, J = 7.64 Hz, 2H, Ph-*H*), 5.69 (d, J = 8.24 Hz, 2H, Ph-*H*), 5.25 (s, 2H, Ph-*H*), 4.55 (s, 4H, -NH_2), 3.62 (-OCH_2, THF), 1.76 (-CH_2, THF) (Fig. S22).

2. XPS full spectrum

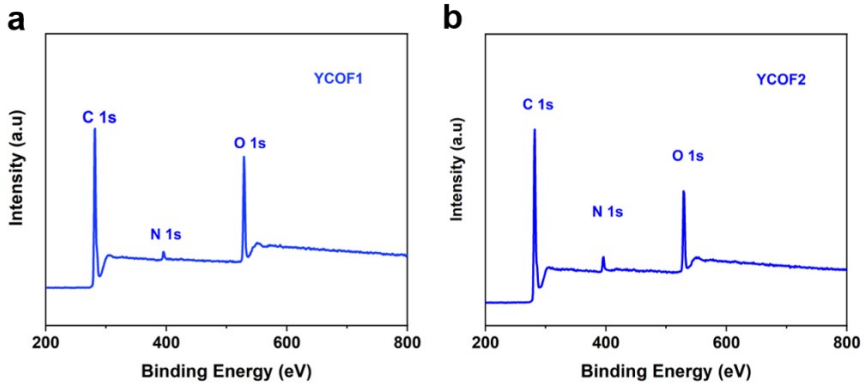

Fig. S1. XPS survey spectra for YCOF1 (a), and YCOF2 (b).

3. SEM images

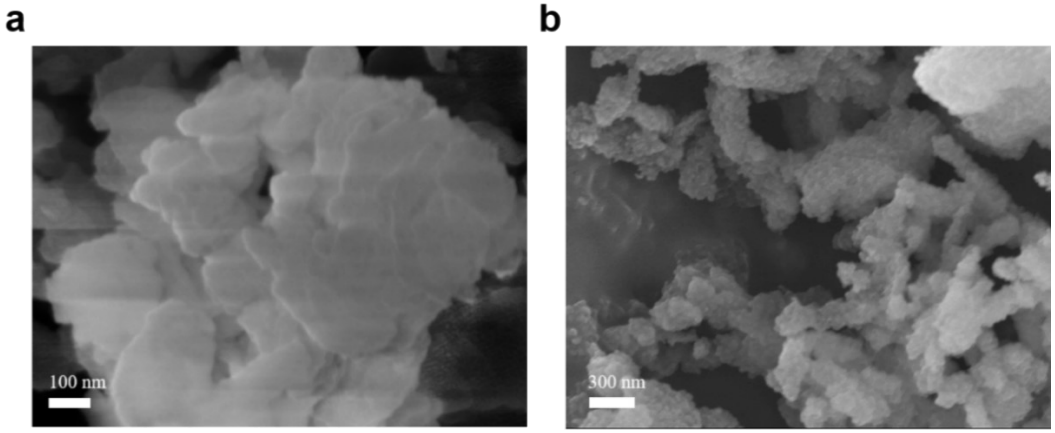

Fig. S2. SEM images of YCOF1 (a), and YCOF2 (b).

4. TGA curve

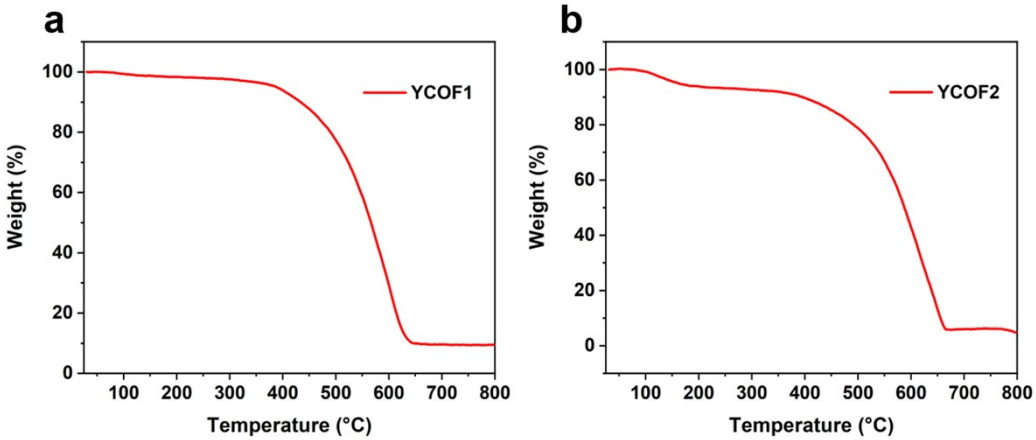

Fig. S3. TGA curves of YCOF1 (a), and YCOF2 (b).

5. PXRD patterns of YCOF1 and YCOF2 soaked in different solvents

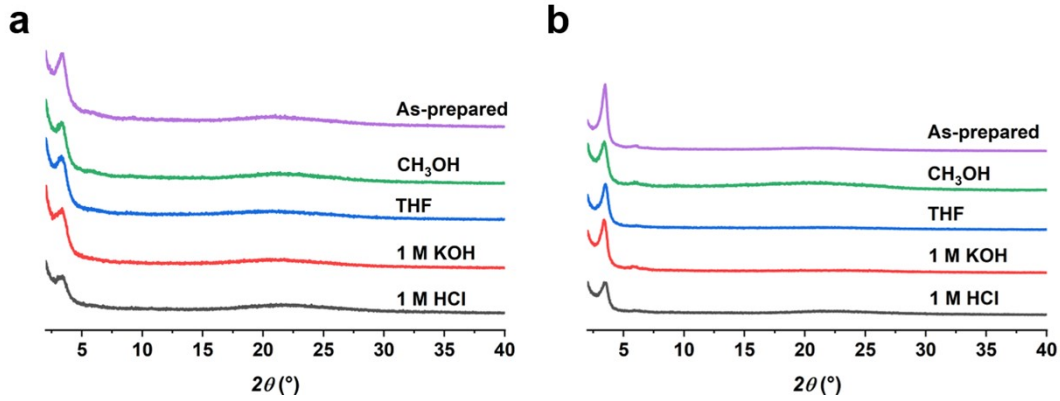

Fig. S4. PXRD patterns of YCOF1 (a), and YCOF2 (b) soaked in different solvents for 24 h at room temperature.

6. CO_2 adsorption heat curve

Clausius–Clapeyron equation:

$$Q_{st} = \frac{RT_1T_2\ln\left(P_2/P_1\right)}{T_2 - T_1} \#6.1$$

R = 8.314 J K^{-1} mol^{-1}, T_1 and T_2 are the adsorption temperatures (K), and P_1 and P_2 are the equilibrium pressures (P/P_0).

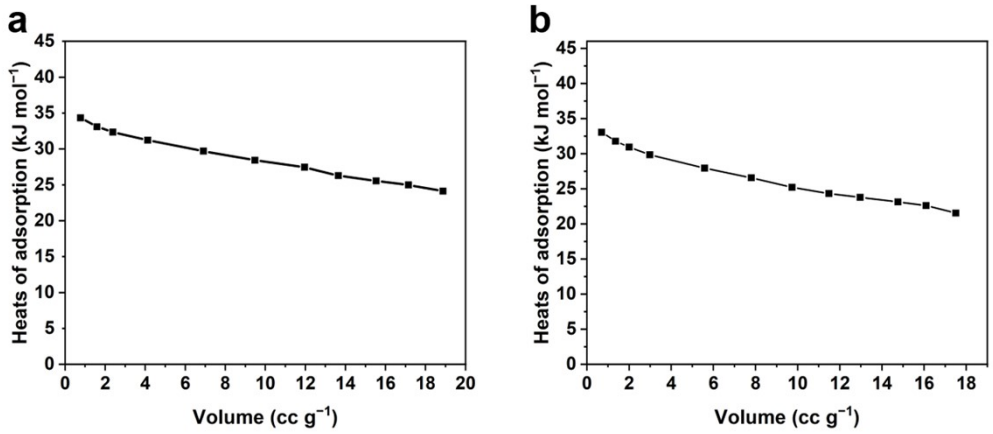

Fig. S5. CO_2 adsorption heat (Q_{st}) of YCOF1 (a), and YCOF2 (b).

7. Fitting parameters of gas adsorption isotherms of YCOF1 and YCOF2

Based on the difference in the adsorption of the two gases, a double Langmuir model was used to fit the adsorption data for CO_2, which exhibits higher adsorption capacity, while a single Langmuir model was employed for N_2, which has a lower adsorption capacity.

The equations for the single and double Langmuir models are as follows:

$$V_{N_2} = \frac{VKP}{1+KP} \#7.1$$

$$V_{CO_2} = \frac{V_1K_1P}{1+K_1P} + \frac{V_2K_2P}{1+K_2P} \#7.2$$

V_{CO_2} is the volume of CO_2 adsorbed by the COFs, V_1, V_2, K_1 and K_2 are model parameters, and P is the applied pressure.

According to the IAST model, the adsorbed phase was assumed to be an ideal solution in equilibrium with the primary adsorption, and the gas obeyed the ideal gas equation of state:

$$\pi_{p_i^0} A = n_i RT \#7.3$$

A is the surface area of the adsorbent, R is the ideal gas constant, and T is the temperature.

The molar amount (n_i) of a component adsorbed by an adsorbent in a gas mixture was:

$$n_i = \int_0^{p_i^0} \frac{n_i(P)}{P} dp \#7.4$$

The isothermal adsorption points of the COFs were fitted according to Equations 7.1 and 7.2 to obtain *K*, *V* values. At equilibrium, the expansion pressures of the two gases were equal.

$$\pi_{p_1^0} = \pi_{p_2^0} \#7.5$$

A, T are constant values. The association of Equations 7.1, 7.2, 7.3, 7.4 and 7.5 yielded 7.6. The relationship between p_1^0 and p_2^0 can be calculated by integration.

$$\int_0^{p_1^0} \left(\frac{V_1 K_1 P}{1 + K_1 P} + \frac{V_2 K_2 P}{1 + K_2 P} \right) dp = \int_0^{p_2^0} \frac{VKP}{1 + KP} dp \#7.6$$

According to Raoult's Law:

$$P_{y_1} = P_1^0 x_1 \#7.7$$

$$P_{y_2} = P_2^0 x_2 \#7.8$$

For binary gas mixtures:

$$x_1 + x_2 = 1 \#7.9$$

$$y_1 + y_2 = 1 \#7.10$$

x_1 and y_1 are the molar fractions of gas component 1 in the adsorbed and gas phases, respectively, and x_2 and y_2 are the molar fractions of gas component 2 in the adsorbed and gas phases, respectively.

Finally, the separation factor S was calculated using the following equation:

$$S = \frac{x_1}{y_1} / \frac{x_2}{y_2} \#7.11$$

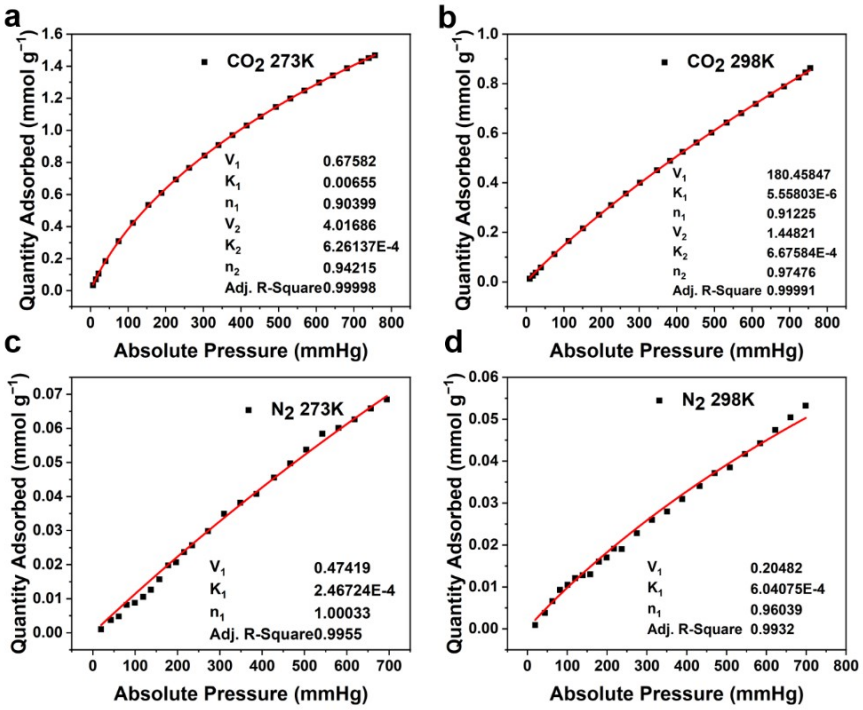

Fig. S6. Langmuir fitting curves and parameters for CO_2 and N_2 adsorptions of YCOF1 at 273 and 298 K.

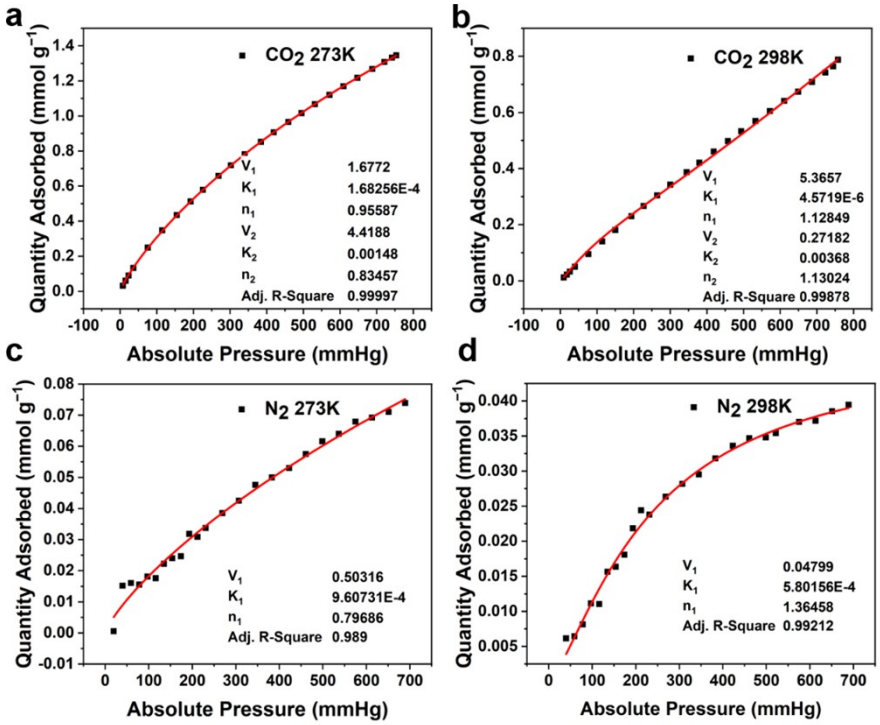

Fig. S7. Langmuir fitting curves and parameters for CO_2 and N_2 adsorptions of YCOF2 at 273 and 298 K.

Table S1 Comparison of CO_2 adsorption and IAST selectivity of selected sorbents

Sample	S_{BET} (m^2 g^{-1})	Capacity (cm^3 g^{-1}) 273 K (298 K)	Selectivity S_{CO_2/N_2} (15:85), 273 K	Ref.
CuBDC-NO_2-a	523	73.92 (53.76)	26.4	[6]
M808	1742	44.8 (30.9)	40	[7]
PCN-161	2516	24.9 (17)	–	[8]
ACOF-1	1176	90.1 (28)	–	[9]
2D-PdPOr-COF	1120	33.85 (19.85)	–	[10]
NH_2-UiO-66	1044	76.14 (53.25)	52.2	[11]
Ni-UiO-66@Br-COF-4	966	86.33 (65.15)	58.9	[11]
DDP600 CTFs	2275	79.47 (49.57)	48.6	[12]
DDP400 CTFs	537	43.35 (−)	185.8	[12]
Me_3TFB-(NH_2)$_2$BD	1624 ± 89	25.4 ± 5.9 (−)	83 ± 11	[13]
3D-HNU5	864	63.53 (−)	–	[14]
YCOF1	559	33.17(19.37)	70.97	**this work**
YCOF2	741	30.32(17.72)	51.9	**this work**

8. Dye adsorption treatment formula

To examine the adsorption kinetic behavior of the samples for the dyes, we employed the most widely used pseudo-first and pseudo-second order kinetic model to analyze the experimental data.

The pseudo-first order kinetic model equation is as follows:

$$\log\left(q_e - q_t\right) = \log\left(c_e\right) - \frac{k_1 t}{2.303} \#8.1$$

The pseudo-second order kinetic model equation is as follows:

$$\frac{t}{q_t} = \frac{1}{k_2 q_e^2} + \frac{t}{q_e} \#8.2$$

q_e and q_t are the adsorption capacity (mg g^{-1}) at equilibrium and at a given time t (min), respectively. k_1 is the rate constant (min^{-1}) for pseudo-first order kinetic model, and k_2 is the rate constant (g mg^{-1} min^{-1}) for pseudo-second order kinetic model.

The time adsorption amount q_t and the equilibrium adsorption amount q_e are calculated as follows:

$$q_t = \frac{(c_0 - c_t)V}{m} \#8.3$$

$$q_e = \frac{(c_0 - c_e)V}{m} \#8.4$$

c_0, c_t and c_e (mg L^{-1}) are the concentrations of the dye at the initial moment, at moment t, and at adsorption equilibrium, respectively. V (mL) is the volume of the solution, and m (mg) is the mass of the adsorbent used.

To further examine the adsorption thermodynamic behavior of the adsorbent for the dye, the two most commonly used adsorption isotherm models were used to analyze the experimental data.

The Langmuir adsorption isotherm model involves monolayer adsorption on a homogeneous surface with the following linearized equation:

$$\frac{c_e}{q_e} = \frac{1}{q_{max}K_L} + \frac{c_e}{q_{max}} \#8.5$$

q_{max} (mg g^{-1}) is the maximum adsorption capacity of the adsorbent, and K_L (L mg^{-1}) is the Langmuir adsorption constant.

The Freundlich adsorption isotherm model assumes that multilayer adsorption occurs on non-uniform surfaces, and the linearized equation can be expressed as follows:

$$\log q_e = \log K_F + \frac{1}{n}\log c_e \#8.6$$

K_F (mg g^{-1} (L mg^{-1})$^{1/n}$) and 1/n are Freundlich isotherm constants, which represent the adsorption amount and adsorption strength, respectively.

Dye removal rate calculation formula:

$$E(100\%) = \frac{C_0 - C_e}{C_0} \times 100\% \#8.7$$

9. Standard curves of MG and ST

To generate the standard curve for the maximum molar absorbance of the dye as a function of concentration, a standard aqueous solution of MG and ST with a concentration of 100 mg L^{-1} was prepared, respectively. Different volumes of the standard solution were then taken and diluted to concentrations of 1.0, 2.0, 3.0, 4.0, 5.0, 6.0, 7.0, 8.0, 9.0, and 10 mg L^{-1}. *UV-Vis* spectra of these solutions were recorded (Fig. S8a and S8c). The absorbances at 617 nm (MG) and 521 nm (ST) were chosen to construct the standard curve (Fig. S8b and S8d).

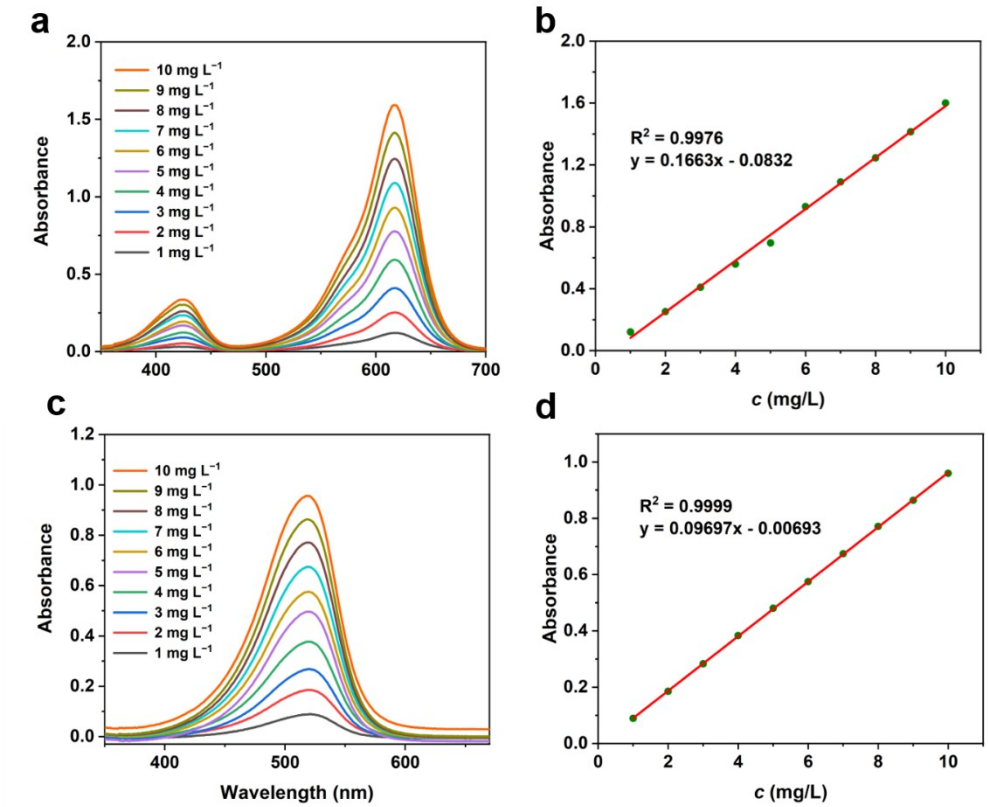

Fig. S8 *UV-Vis* spectra and standard curves of MG (a, b), and ST (c, d).

10. Kinetic and thermodynamic fitting parameters

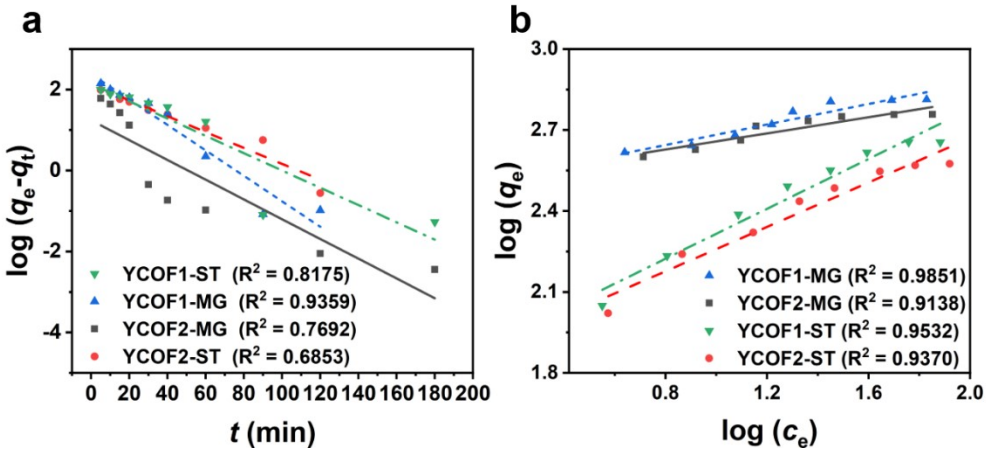

Fig. S9. Fitting pseudo-first-order kinetic curves (a), and Freundlich (b) adsorption isotherms of YCOF1 and YCOF2.

Table S2 Adsorption kinetic model fitting parameters of YCOF1 and YCOF2 for the dyes

Dye	Adsorbent	Pseudo-I-order model			Pseudo-II-order model		
		k_1 (h^{-1})	q_e (mg g^{-1})	R^2	k_2 (g mg^{-1} h^{-1})	q_e (mg g^{-1})	R^2
MG	YCOF1	0.0723	238.67	0.9359	0.00068	425.53	0.9997
	YCOF2	0.0562	172.13	0.7692	0.0034	400	0.9999
ST	YCOF1	0.0492	136.46	0.8175	0.00056	227.79	0.9983
	YCOF2	0.0451	133.20	0.6853	0.00336	200	0.9997

Table S3 Adsorption thermodynamic model fitting parameters of YCOF1 and YCOF2 for the dyes

Dye	Adsorbent	Langmuir isotherm model			Freundlich isotherm model		
		k_L (L mg^{-1})	q_{max} (mg g^{-1})	R^2	k_F (mg g^{-1} (L $mg^{-1})^{1/n}$)	1/n	R^2
MG	YCOF1	0.24	694.44	0.9983	310.66	0.19	0.9851
	YCOF2	0.36	598.80	0.9995	321.90	0.15	0.9138
ST	YCOF1	0.75	510.20	0.9969	71.41	0.46	0.9532
	YCOF2	0.84	414.92	0.9935	70.45	0.41	0.9370

Table S4 Summary of the adsorption capacities of two dyes in the selected literatures and this paper

Dyes	Adsorbents	Removal capacity (mg g^{-1})	References
MG	COF-TPDD-COOH	128.64	[15]
MG	CPCMERI-2020	350	[16]

MG	AMCD-ZIF/PVC-M	476	[17]
MG	AMCD-ZIF	2500	[17]
MG	Rt/MAn	513	[18]
MG	Ag-MOF	809.71	[19]
MG	TPE-Por-COF	1428.57	[20]
MG	GSA	1375.58	[21]
MG	Cage-COF-TP	1805	[22]
MG	TpStb-SO_3Na	5857	[23]
MG	YCOF1	650.14	**this work**
MG	YCOF2	572.95	**this work**
ST	PVAL/PANI/MMT	57.0	[24]
ST	GBD	165.63	[25]
ST	MIL-101(Cr)-SO_3H	425.5	[26]
ST	Bio-Ox@CPTMS@Melamine/Poly (AA)	711.340	[27]
ST	WEPS-BTA	1036.7	[28]
ST	TpPa-COOH	1135	[29]
ST	YCOF1	451.92	**this work**
ST	YCOF2	375.67	**this work**

11. Selective adsorption experiments

MG (25 mg L^{-1}) was mixed with equal amounts of ST (25 mg L^{-1}) to form a binary system. To two 20 mL of the mixed solution were added 1 mg of YCOF1 and YCOF2, respectively. Their *UV-Vis* spectra were measured after reaching adsorption equilibrium. The results showed that the removal rates of MG and ST by YCOF1 were 81.95% and 50.68%, and the removal rates of MG and ST by YCOF2 were 82.26% and 45.68%, respectively.

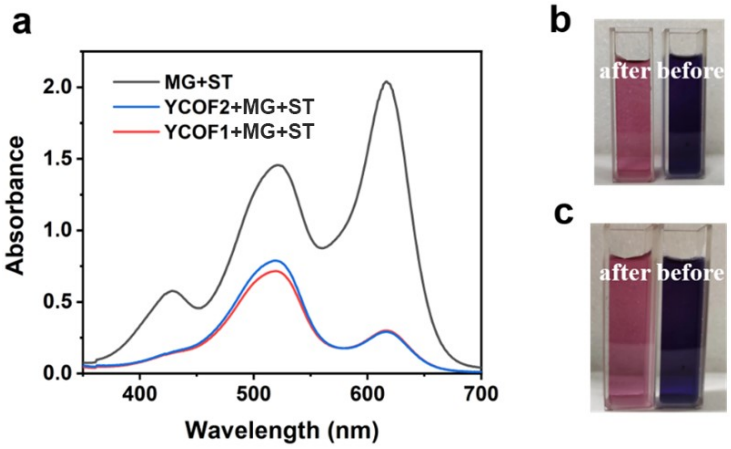

Fig. S10. *UV-Vis* spectra of YCOF1 and YCOF2 when reaching adsorption equilibrium for binary dye mixtures (a); Comparison pictures of dye solutions before and after dye adsorption by YCOF1 (b), and YCOF2 (c).

12. The simulation 3D structures of MG and ST

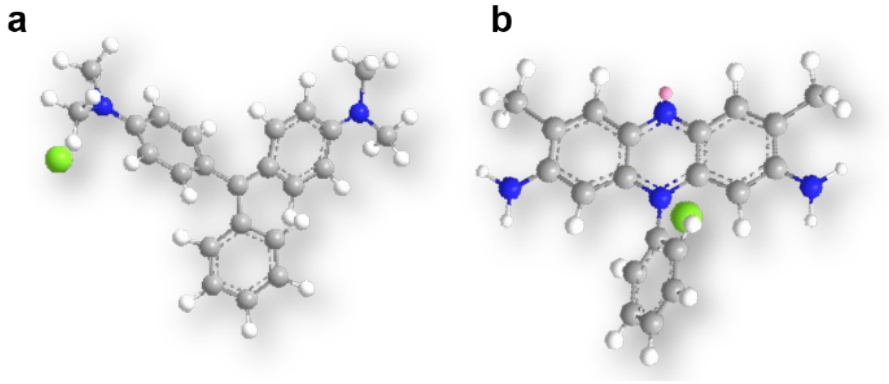

Fig. S11. 3D structures of MG (a) and ST molecule (b): Carbon (gray), hydrogen (white), nitrogen (blue), chlorine (green), lone pair (pink).

13. Cycle regeneration experiment of YCOF1 and YCOF2

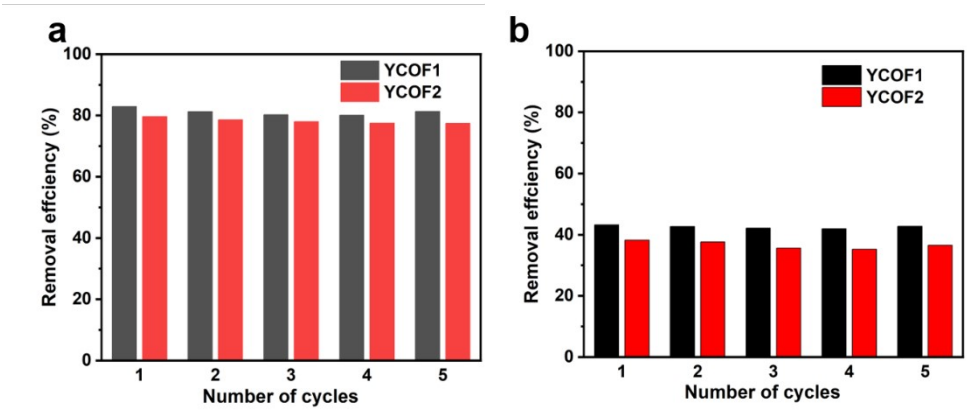

Fig. S12. The recyclability of YCOF1 and YCOF2 loaded with dyes MG (a) and ST (b).

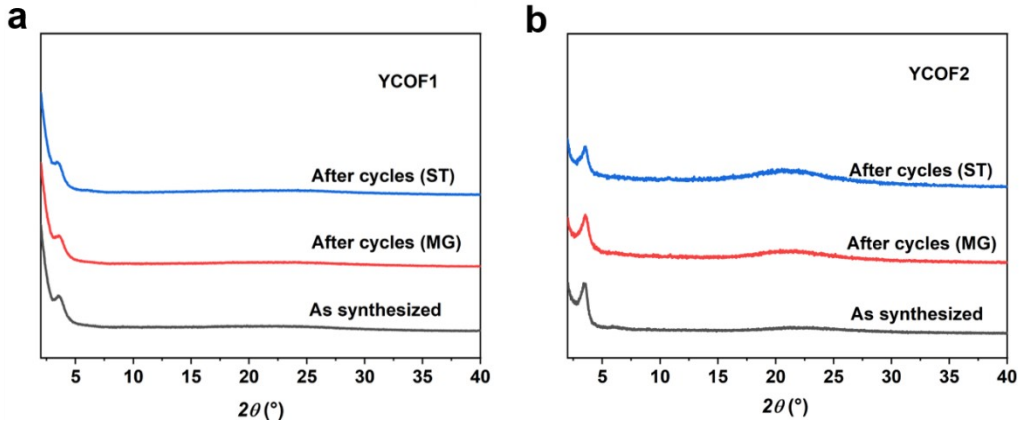

Fig. S13. PXRD patterns of YCOF1 (a), and YCOF2 (b) after 5 adsorption cycles.

14. NMR spectra

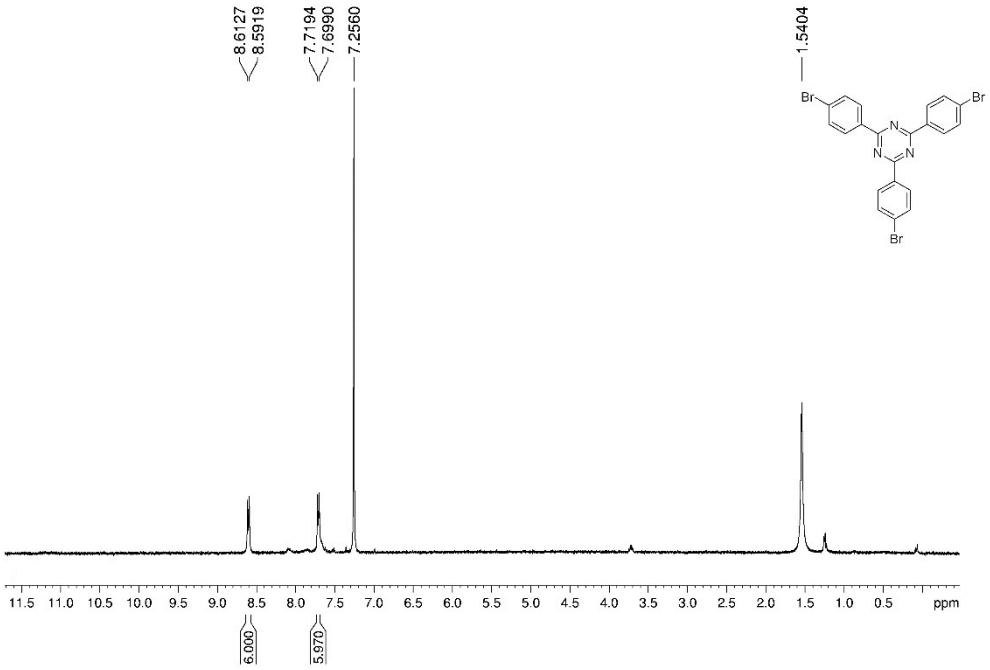

Fig. S14. ^{1}H NMR (400 MHz, $CDCl_3$) of 2,4,6-tris(4-bromophenyl)-1,3,5-triazine.

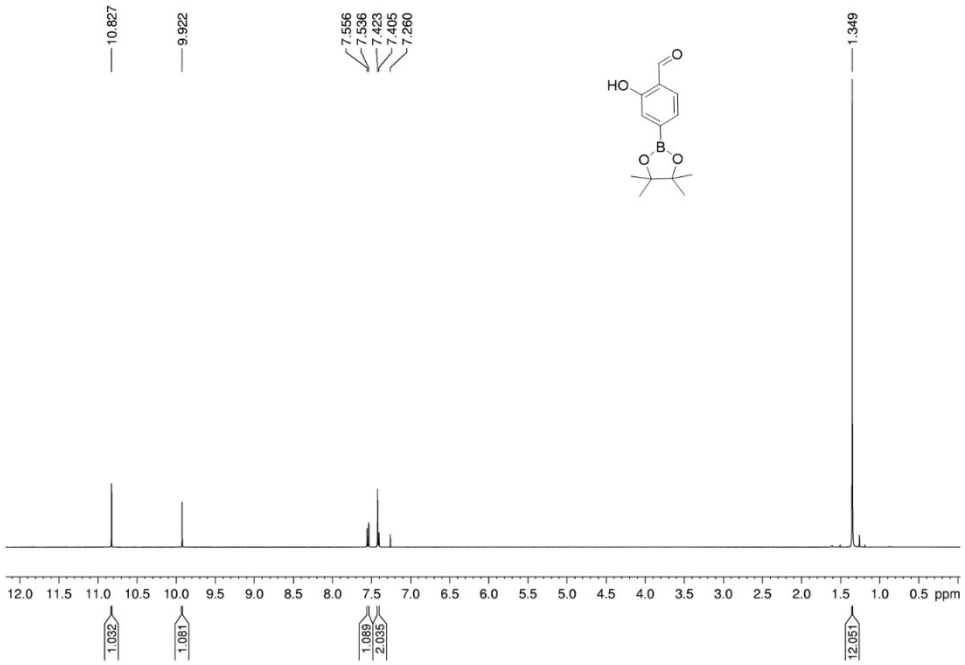

Fig. S15. ^{1}H NMR (400 MHz, $CDCl_3$) of compound **a**.

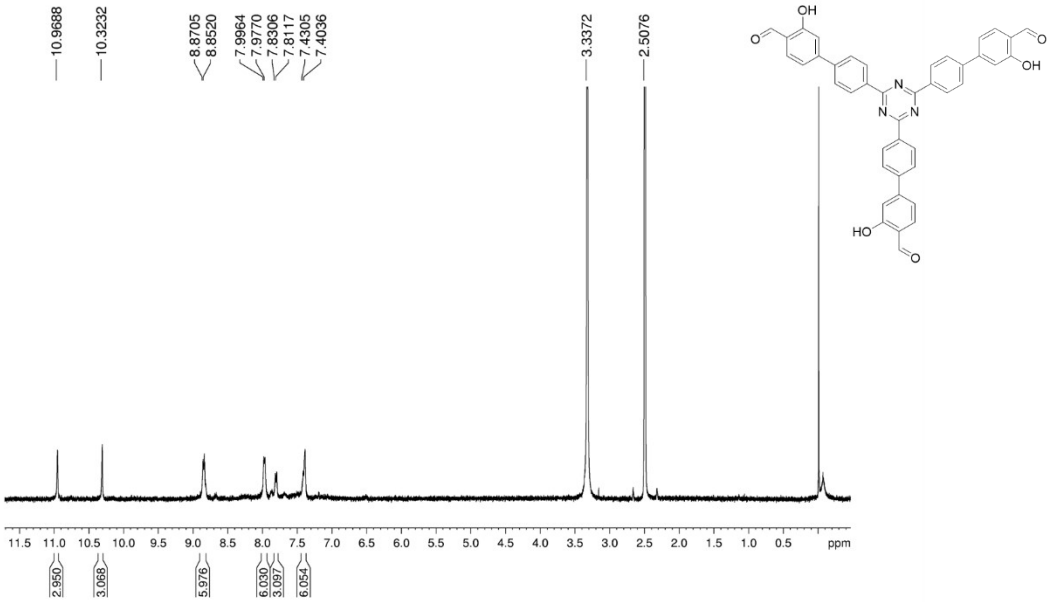

Fig. S16. ^{1}H NMR (400 MHz, DMSO-d_6) of 4',4''',4''''-(1,3,5-triazine-2,4,6-triyl)tris(3-hydroxy-[1,1'-biphenyl]-4-carbaldehyde).

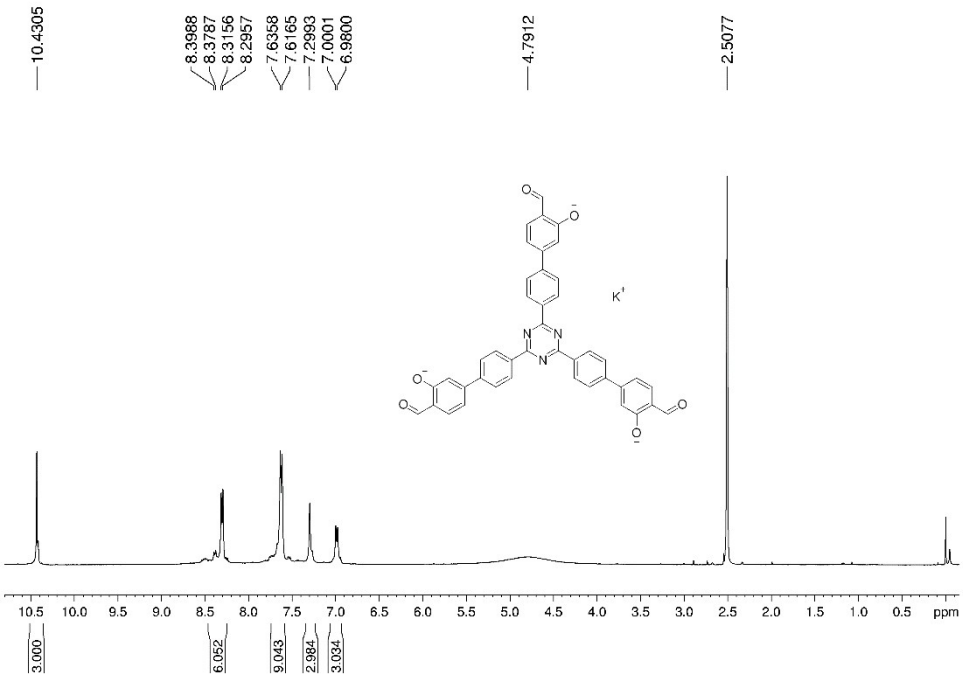

Fig. S17. ^{1}H NMR (400 MHz, DMSO-d_6) of 4',4''',4''''-(1,3,5-triazine-2,4,6-triyl)tris(3-hydroxy-[1,1'-biphenyl]-4-carbaldehyde) treated with KOH.

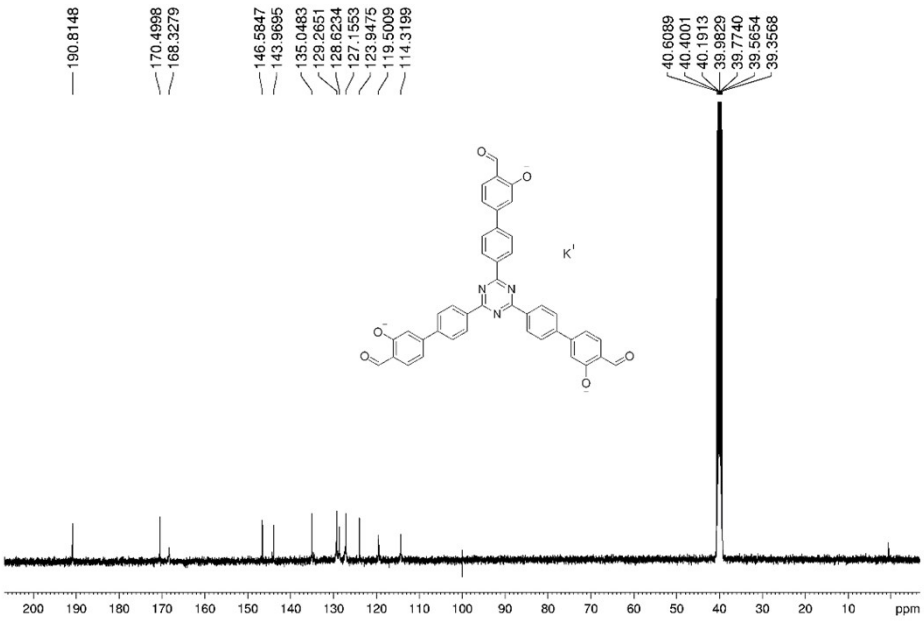

Fig. S18. ^{13}C NMR (400 MHz, DMSO-d_6) of 4',4''',4''''-(1,3,5-triazine-2,4,6-triyl)tris(3-hydroxy-[1,1'-biphenyl]-4-carbaldehyde) treated with KOH.

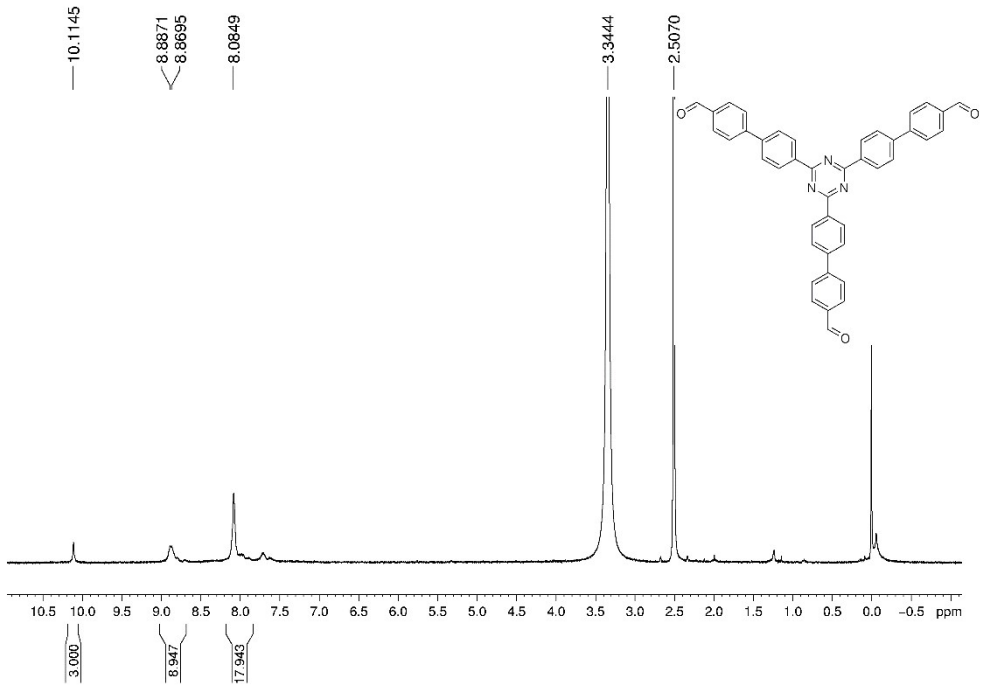

Fig. S19. ^{1}H NMR (400 MHz, DMSO-d_6) of 4',4''',4''''-(1,3,5-triazine-2,4,6-triyl)tris([1,1'-biphenyl]-4-carbaldehyde).

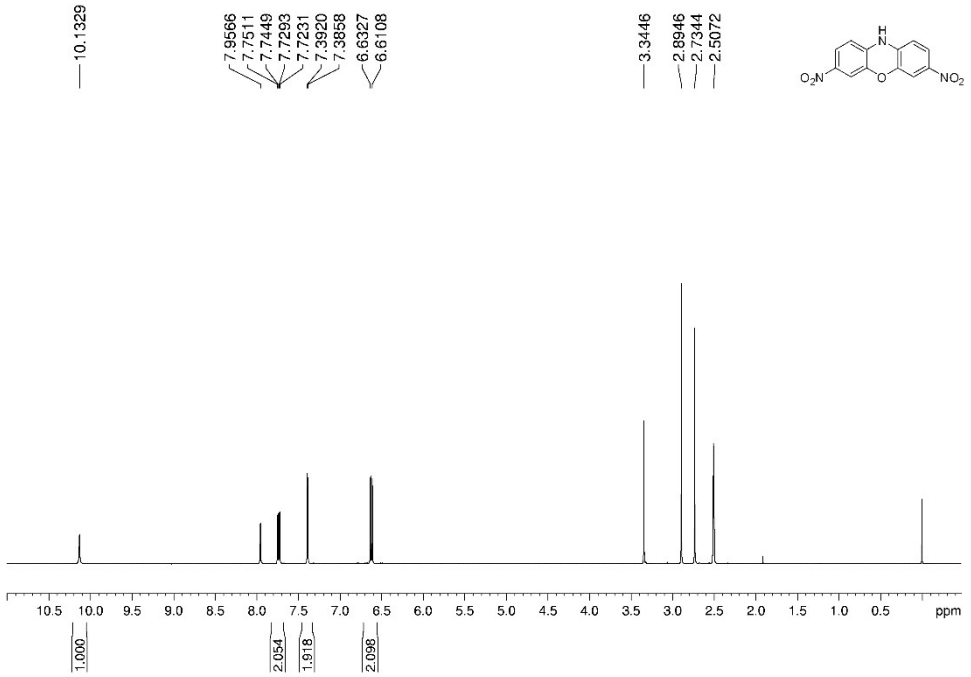

Fig. S20. ^{1}H NMR (400 MHz, DMSO-d_6) of compound **b**.

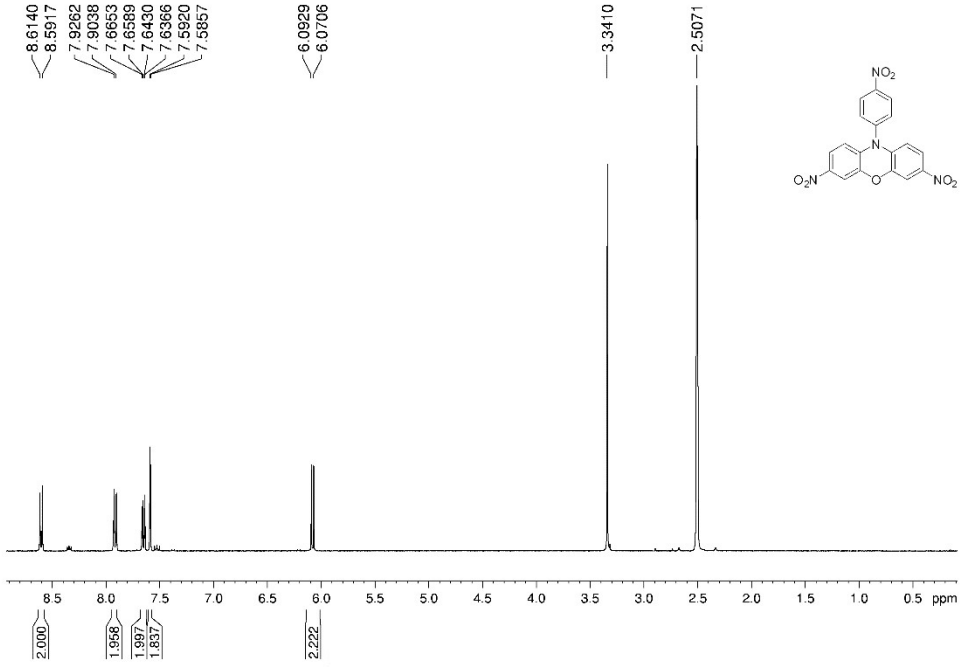

Fig. S21. ^{1}H NMR (400 MHz, DMSO-d_6) of compound **c**.

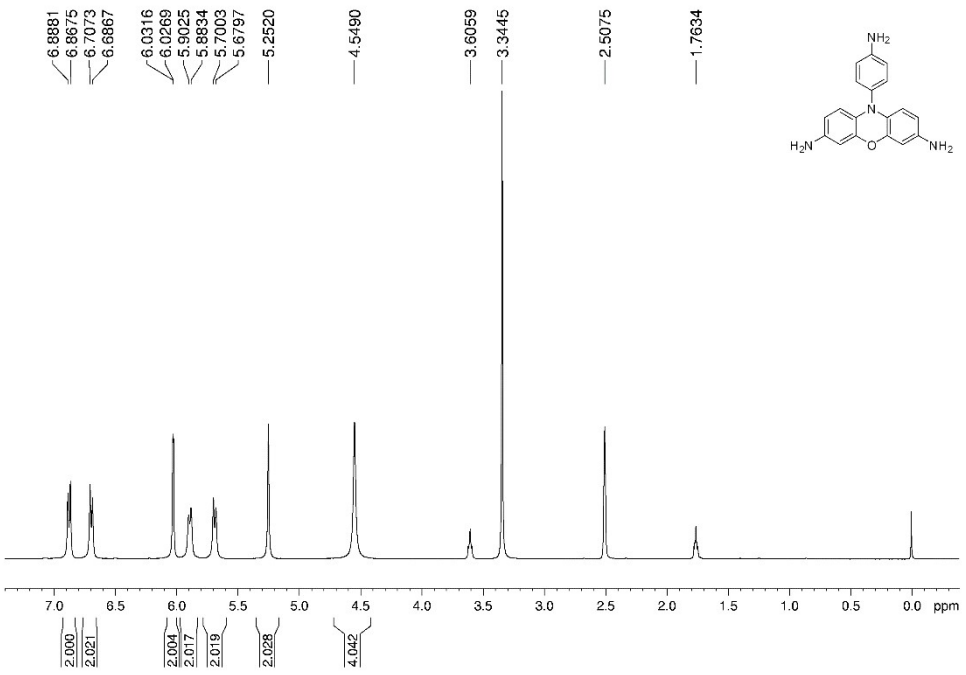

Fig. S22. ^{1}H NMR (400 MHz, DMSO-d_6) of 10- (4-aminophenyl)-3,7-phenoxazinediamine.

15. References

1. T. He, Z. Huang, S. Yuan, X.-L. Lv, X.-J. Kong, X. Zou, H.-C. Zhou and J.-R. Li, *J. Am.*

Chem. Soc., 2020, **142**, 13491-13499.
2. D. Schwarz, Y. S. Kochergin, A. Acharjya, A. Ichangi, M. V. Opanasenko, J. Čejka, U. Lappan, P. Arki, J. He, J. Schmidt, P. Nachtigall, A. Thomas, J. Tarábek and M. J. Bojdys, *Chem. Eur. J.*, 2017, **23**, 13023-13027.
3. F. Mamiya, N. Ousaka and E. Yashima, *Angew. Chem. Int. Ed.*, 2015, **54**, 14442-14446.
4. S. Bi, Z. Zhang, F. Meng, D. Wu, J.-S. Chen and F. Zhang, *Angew. Chem. Int. Ed.*, 2022, **61**, e202111627.
5. L. A. Farmer, Z. Wu, J.-F. Poon, O. Zilka, S. M. Lorenz, S. Huehn, B. Proneth, M. Conrad and D. A. Pratt, *J. Am. Chem. Soc.*, 2022, **144**, 14706-14721.
6. H. Cui, Y. Ye, T. Liu, Z. A. Alothman, O. Alduhaish, R.-B. Lin and B. Chen, *Inorg. Chem.*, 2020, **59**, 17143-17148.
7. J. M. Park, D. K. Yoo and S. H. Jhung, *Chem. Eng. J.*, 2020, **402**, 126254.
8. U. S. F. Arrozi, V. Bon, S. Krause, T. Lübken, M. S. Weiss, I. Senkovska and S. Kaskel, *Inorg. Chem.*, 2020, **59**, 350-359.
9. Z. Li, X. Feng, Y. Zou, Y. Zhang, H. Xia, X. Liu and Y. Mu, *Chem. Commun.*, 2014, **50**, 13825-13828.
10. Y. Meng, Y. Luo, J.-L. Shi, H. Ding, X. Lang, W. Chen, A. Zheng, J. Sun and C. Wang, *Angew. Chem. Int. Ed.*, 2020, **59**, 3624-3629.
11. J. Wang, L. Wang, Y. Wang, F. Yang, J. Li, X. Guan, J. Zong, F. Zhou, J. Huang and Y.-N. Liu, *Chem. Eng. J.*, 2022, **438**, 135555.
12. M. Mahato, S. Nam, R. Tabassian, S. Oh, V. H. Nguyen and I.-K. Oh, *Adv. Funct. Mater.*, 2022, **32**, 2107442.
13. E. Dautzenberg, G. Li and L. C. P. M. de Smet, *ACS Appl. Mater. Interfaces*, 2023, **15**, 5118-5127.
14. P. Guan, J. Qiu, Y. Zhao, H. Wang, Z. Li, Y. Shi and J. Wang, *Chem. Commun.*, 2019, **55**, 12459-12462.
15. S. Liu, L. Yang, T. Quan, L. Deng, D. Wang, K. Zhang, L. Wang, J. Wang, F. Ke, X. Li and D. Gao, *Sep. Purif. Technol.*, 2022, **288**, 120673.
16. D. Dey, A. Mondal, S. Nag, U. Mondal, H. Hirani and P. Banerjee, *New J. Chem.*, 2021, **45**, 5165-5175.
17. A. Jaafar, S. El-Husseini, C. Platas-Iglesias and R. A. Bilbeisi, *J. Environ. Chem. Eng.*, 2022, **10**, 108019.
18. H. S. Ramadan, R. A. M. Ali, M. Mobarak, M. Badawi, A. Q. Selim, E. A. Mohamed, A. Bonilla-Petriciolet and M. K. Seliem, *Chem. Eng. J.*, 2021, **426**, 131890.
19. M. M. Aljohani, S. D. Al-Qahtani, M. Alshareef, M. G. El-Desouky, A. A. El-Bindary, N. M. El-Metwaly and M. A. El-Bindary, *Process Saf. Environ. Prot.*, 2023, **172**, 395-407.
20. S. Chang, W. Xie, C. Yao, G. Xu, S. Zhang, Y. Xu and X. Ding, *J. Solid State Chem.*, 2021, **304**, 122577.
21. Y. Wen, Z. Xie, S. Xue, W. Li, H. Ye, W. Shi and Y. Liu, *J. Hazard. Mater.*, 2022, **426**, 127799.
22. M. Li, J. Ma, B. Pan and J. Wang, *ACS Appl. Mater. Interfaces*, 2022, **14**, 57180-57188.
23. R. Li, X. Tang, J. Wu, K. Zhang, Q. Zhang, J. Wang, J. Zheng, S. Zheng, J. Fan, W. Zhang, X. Li and S. Cai, *Chem. Eng. J.*, 2023, **464**, 142706.
24. W. Lyu, J. Li, M. Trchová, G. Wang, Y. Liao, P. Bober and J. Stejskal, *J. Hazard. Mater.*,

2022, **435**, 129004.
25. C. Roy, A. Dutta, M. Mahapatra, M. Karmakar, J. S. D. Roy, M. Mitra, P. K. Chattopadhyay and N. R. Singha, *J. Hazard. Mater.*, 2019, **369**, 199-213.
26. X. Zhao, K. Wang, Z. Gao, H. Gao, Z. Xie, X. Du and H. Huang, *Ind. Eng. Chem. Res.*, 2017, **56**, 4496-4501.
27. E. Mosaffa, R. I. Patel, A. M. Purohit, B. B. Basak and A. Banerjee, *J. Polym. Environ.*, 2023, **31**, 2486-2503.
28. W. Li, Z. Xie, S. Xue, H. Ye, M. Liu, W. Shi and Y. Liu, *Sep. Purif. Technol.*, 2021, **276**, 119435.
29. B. Dong, W.-J. Wang, S.-C. Xi, D.-Y. Wang and R. Wang, *Chem. Eur. J.*, 2021, **27**, 2692-2698.